ARMY RESEARCH LABORATORY

A Slotted-Waveguide Array for High-Power Microwave Transmission

William Coburn, Marc Litz, Joseph Miletta, Neal Tesny, Lillian Dilks, Charles Brown, and Benson King

ARL-TR-2331   January 2001

20010314 082

Army Research Laboratory

Adelphi, MD 20783-1197

A Slotted-Waveguide Array for High-Power Microwave Transmission

William Coburn, Marc Litz, Joseph Miletta, Neal Tesny, Lillian Dilks, Charles Brown, and Benson King
Sensors and Electron Devices Directorate

Abstract

Directive antennas are required for the development of high-power microwave (HPM) transmission system concepts. The type of system considered includes a single HPM source with waveguide output, the antenna, and the control/support equipment integrated onto a ground-mobile platform. A parabolic reflector with a custom-designed horn feed has been demonstrated as one antenna option that allows direct connection to the HPM source waveguide output. An alternative approach to reflector antennas is desired, so a slotted-waveguide array was selected to meet the operational requirements. The array design is modular (with four symmetric modules) to ease fabrication and to maximize transportability and repairability. A rectangular waveguide corporate-feed network is used to minimize the antenna subsystem volume (i.e., depth) and allow the HPM source to be integrated into the feed structure. An S-band array and feed structure were fabricated and assembled for laboratory evaluation. The array was fabricated from WR-284 copper waveguide with brass end caps to a ± 5-mil tolerance. The array design, fabrication, assembly, and testing are discussed. Preliminary test data for a single module of the four-module full array are presented. As expected, the array as fabricated requires "fine-tuning" to optimize performance. Empirical results will be used to evaluate design alternatives appropriate for particular HPM applications.

Contents

Figures

1. Introduction

A conceptual high-power microwave (HPM) transmission system includes a single HPM source with waveguide output, the antenna subsystem, and the control/support equipment integrated onto a ground-mobile platform. The U.S. Army Research Laboratory (ARL) is exploring technologies in each of these areas to investigate HPM concepts for future Army applications. In particular, the relativistic klystron (or Reltron) microwave tube represents a compact, lightweight HPM source with a narrow (i.e., <10 percent) frequency bandwidth (BW). Directive antennas are required in the development of such HPM systems for mobile applications. A parabolic reflector with a custom-designed horn feed is one antenna option that allows direct connection to the HPM source waveguide output. An alternative approach to reflector antennas is desired, so slot array antennas have been investigated.

For large arrays, identical row waveguide elements are attractive to minimize cost and complexity in the antenna design, fabrication, and assembly. The longitudinal (shunt) slot resonant array with cosine-squared "on-a-pedestal" array taper was selected to meet the operational requirements. This broadside array uses resonant element spacing and so has a narrow frequency BW that is comparable to that of the Reltron. The array design is modular (with four symmetric modules) for ease of fabrication and to maximize transportability and repairability. A rectangular waveguide feed network is used to minimize the antenna subsystem volume (i.e., depth). The Reltron is integrated into the feed structure so that the HPM source and antenna can be mounted on a gimbal base for mechanical pointing. An S-band array is fabricated from a basic design for empirical test and evaluation. The results will be used to refine the array design for optimum performance in a specific application.

The slotted-waveguide modules, corporate-feed waveguide, and source interface are fabricated from WR-284 (S-band) copper waveguide with brass end caps and 0.080 ± 0.005-in. (80 ± 5 mil) wall thickness. It is important to note that WR-284 has exterior dimensions such that the height is half the width (i.e., half-height). The interior dimensions are not exactly a half-height waveguide, having an inside width, $a = 2.84$ in. and inside height, $b = 1.34$ in. Numerically controlled (NC) milling operations were used to fabricate the slotted waveguide to strict tolerance (±5 mil). The S-band array design, fabrication, assembly, and testing are discussed. Preliminary test data for a single module of the four-module full array are presented to establish an empirical baseline for the array as fabricated from the basic design. Analytical results for an idealized array are in qualitative agreement with the measured data. The slot array resonant frequency is shifted from the design frequency, because of perturbation of the resonant slot length.

1

The results indicate that selected slot elements would require tuning to optimize performance. Tunable elements for impedance matching could also be used to maximize the efficiency of the array over narrow frequency bands.

2. Array Design

ARL is investigating array antennas suitable for high-power operation at *S*- and *L*-band frequencies. These antenna systems are required to interface with a Reltron HPM source that has a single rectangular waveguide output. Peak-pulsed power levels are greater than 25 MW with full pulsewidth (PW) about 2 μs. Pulse repetition frequency (PRF) is several hundred hertz and is limited by a maximum duty factor (DF) of roughly 0.1 percent, corresponding to average power-handling requirements greater than 10 kW. A study was conducted to identify and design a suitable radiating system with high gain (i.e., >20 dBi) and a side-lobe level (SLL) of 20 dB. That is, the radiation pattern is a pencil beam with side-lobe amplitudes at least 20 dB less than that of the main beam. The approach was to meet the antenna operational requirements by modifying a basic design based on empirical results. The basic design involved many simplifying assumptions, so an *S*-band array was fabricated for test and evaluation.

The nominal performance requirements of the antenna system are shown in table 1 with a 1-dB gain margin. Vertical polarization (with respect to the ground) with at least 40-dB cross-polarized isolation is required on boresight. In addition, the antenna size, weight, and complexity are minimized for potential use on ground-mobile vehicles. The antenna array design should be modular for ease of transportation, deployment, maintenance, and power handling. ARL conducted a study to evaluate candidate approaches for meeting the HPM antenna requirements. Secondary objectives were to identify design alternatives with the potential to reduce the array's size and weight.

2.1 Design Study

The primary attributes of an antenna array are its directive gain, antenna efficiency or realized gain, SLL, frequency BW, and physical size. The array's physical size is chosen to yield the desired gain plus design margin (i.e., 31 dBi for a 30-dBi desired gain), given an estimate of the excitation

Table 1. Nominal performance specifications for HPM antenna arrays.

Frequency range (GHz)	Frequency BW (%)	Gain (dBi)	SLL (dB)	Peak-power level (MW)	Full beamwidth (°)
L-band 1.25–1.35	≥ 7.7	≥ 30	≥ 20	≥ 50	≤ 6
S-band 2.7–2.9	≥ 7.1	≥ 30	≥ 20	≥ 25	≤ 6

efficiency factor. The following observations are generally true, since the physical and electrical attributes of antenna arrays are interrelated:

- Increasing the antenna gain requires an increase in the SLL, a decrease in BW, or an increase in the physical size.

- Increasing the antenna frequency BW requires that gain or SLL be sacrificed or physical size increased to accommodate a better array excitation.

- Reducing the antenna SLL requires either a decrease in gain or BW or an increase in physical size so that a tapered array excitation can be used to reduce the SLL.

- Reducing the physical size results in decreased gain, increased SLL, or decreased BW. However, reducing the physical size is sometimes possible with the use of a more sensitive array taper that reduces BW while maintaining the same gain and SLL.

In this design effort, we chose the physical size to exceed the gain requirement (plus margin) and the array excitation taper to meet the SLL requirement. In this approach, the desired frequency BW could not be obtained without an increase in the overall size and complexity of the array.

We considered two basic types of slotted-waveguide antennas for meeting the performance specifications, the resonant array and the traveling-wave (or nonresonant) array. The nonresonant array advantages are a wider frequency BW than the resonant array advantages. However, the disadvantages are severe in that terminating loads are required to absorb power (i.e., reduced efficiency), and the main-beam direction depends on the operating frequency. The resonant array is terminated in a short circuit so that power is not wasted in a load. The main beam is normal to the array but has a narrower frequency BW compared to the nonresonant array frequency BW. The realized gain versus frequency can also depend on characteristics of the radiating elements. This is called the "pattern" BW, which is centered on the frequency for peak radiation and defined by the half-power (i.e., 3 dB) points. The analytical voltage standing-wave ratio (VSWR) assumes that the input impedance is a pure resistance (at the design frequency), so the frequency BW can also be limited by the impedance mismatch caused by a nonzero input reactance. This is called the "impedance" BW, which is centered on the minimum VSWR and defined by a VSWR less than twice the minimum. The combination of the pattern and impedance BW then determines the array frequency BW, depending on the maximum allowable VSWR. The final design indicates a compromise in frequency BW to meet the other performance specifications.

The antenna system found to best meet the operational requirements is a resonant array of slotted-waveguide antennas with a corporate-feed waveguide [1,2]. This particular type is a resonant array of four near-center-fed modules that contain longitudinal slots as will be discussed in section 2.2. The theory of such antenna systems is well-founded, and mutual coupling effects are often neglected for this type of slotted-waveguide array
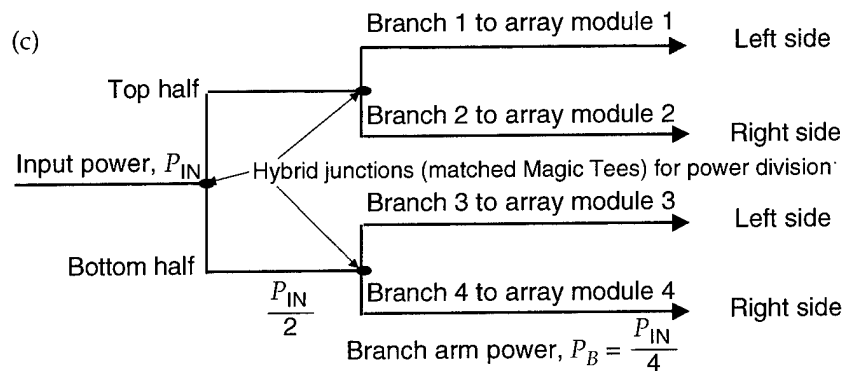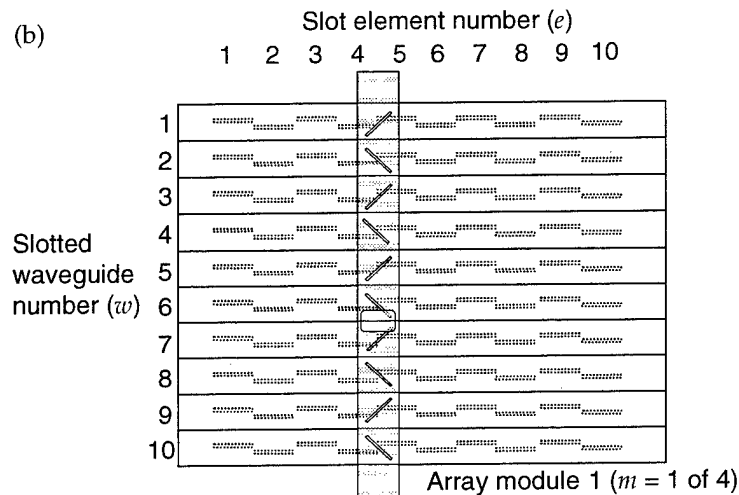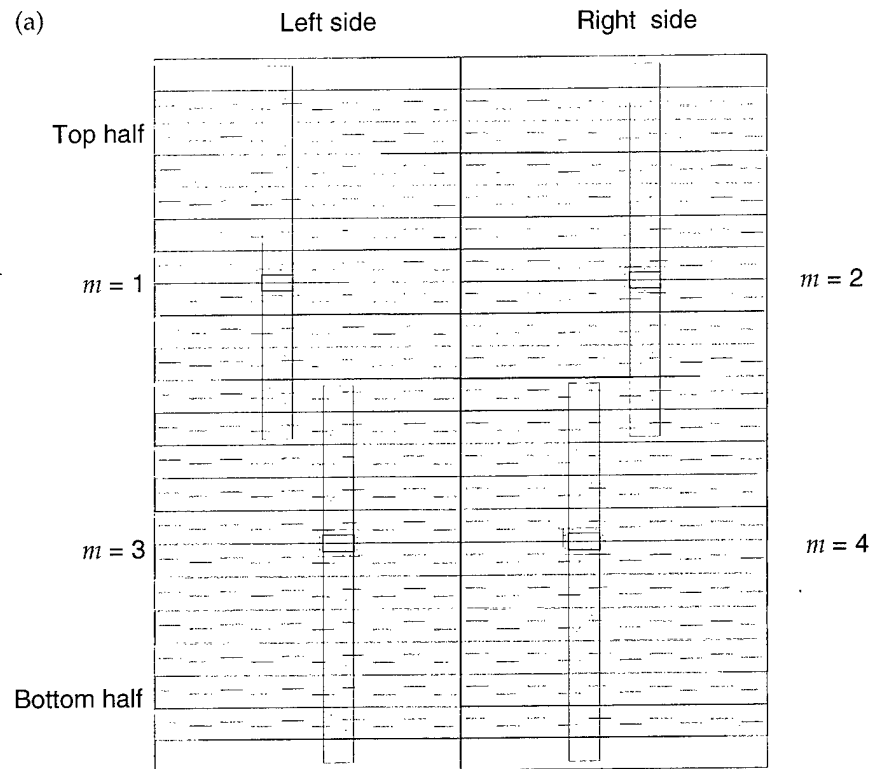
[3–8]. Relatively large arrays have been constructed, and mechanical factors affecting performance have been previously investigated [9–12]. The analysis-based design resulted in an array with a "cosine squared on a pedestal" excitation. A pedestal height of 0.177 provides an SLL of 20 dB and an aperture efficiency of approximately 90 percent [13,14]. Hybrid waveguide junctions (or "Magic Tees") are used in the feed network that equally distributes power to the corporate-feed waveguide of each module. Analysis indicates that additional modules (up to 16) can increase the array frequency BW but may lead to complex feed structures, which require nonuniform distribution of the input power [2].

2.2 S-Band Array

The generalized antenna-structure rear view is shown in figure 1(a), indicating the arrangement of the corporate-feed waveguide and the module numbering convention (i.e., ordered clockwise in the rear view). The coupling slots in the rear of the slotted-waveguide arms and the radiating slots in the front face of the waveguide are shown with solid lines rather than with dotted lines for these hidden array features. A single array module is shown in figure 1(b), where the coupling slots are shown with solid lines rather than with hidden lines. The array nomenclature is as indicated for each array module ($m = 1 - 4$), where $e = 1 - 10$ refers to the slot element number and $w = 1 - 10$ refers to the waveguide number. In each module, the last slot element ($e = 10$) and the last waveguide ($w = 10$) are at the array center. Nonfunctional "dummy" waveguide (or equivalent) is included at the top and bottom of the array as shown in figure 1(a) to provide a mounting surface and closure for the feed waveguide. Therefore, the array is not square, having a total width of roughly 5.1 ft and a total height of 5.6 ft. In this orientation (with respect to the ground), the polarization is vertical as in an array of vertical dipole antennas.

Power is equally distributed to the feed arms of the four modules as shown schematically in figure 1(c). The corporate-feed waveguide then distributes power to the waveguide arms that contain the slot elements according to the tapered excitation. The impedance analysis of the corporate-feed arm is independent of the location of the feed waveguide along the waveguide arms, although an even number of slot elements on each side is required so that the reactive impedance cancels. Further, the input impedance at the module (i.e., at the WR-284 rectangular flange) is roughly independent of the location on the feed-arm waveguide for an even number of coupling slots on each side of this input. The physical arrangement of the feed-arm sections is chosen for flexibility in configuring the equal length interface to a single-source waveguide. The effect of conductor losses on the array efficiency is not considered in the design phase, since these losses should be small compared to mismatch losses.

Figure 1. Slotted waveguide array (a) structure (rear view) with slot elements not hidden, (b) module rear view (not to scale) showing nomenclature, and (c) feed-structure schematic diagram with equal power distribution.

(a)

Left side   Right side

Top half

$m = 1$ $m = 2$

$m = 3$ $m = 4$

Bottom half

(b)

Slot element number (e)

1 2 3 4 5 6 7 8 9 10

Slotted waveguide number (w)

1
2
3
4
5
6
7
8
9
10

Array module 1 ($m = 1$ of 4)

(c)

Branch 1 to array module 1   Left side

Top half

Branch 2 to array module 2   Right side

Input power, P_{IN} Hybrid junctions (matched Magic Tees) for power division

Branch 3 to array module 3   Left side

Bottom half

$\dfrac{P_{IN}}{2}$ Branch 4 to array module 4   Right side

Branch arm power, $P_B = \dfrac{P_{IN}}{4}$

6

2.2.1 Array Modules

The radiating elements are half-wavelength longitudinal slots in the broad-face of WR-284 copper waveguide. The design center frequency, $f_0 = c/\lambda_0 = 2.86$ GHz, corresponds to free-space wavelength, $\lambda_0 = 10.5$ cm. The center frequency then determines the slot length $l = \lambda_0/2 = 5.25$ cm, which is at resonant spacing, $d_s = \lambda_g/2$, for the air-filled guide wavelength, λ_g, corresponding to λ_0. The slots are offset from the broadface centerline as shown in figure 2(a), with the smallest displacements at the array edges and steadily increasing toward the center. This provides the tapered array excitation along the waveguide axis corresponding to the H-plane (i.e., horizontal or azimuthal) radiation pattern. The waveguide is terminated at each end with end caps (i.e., short-circuit terminations) that are located at $\lambda_g/4$ from the last slots, which transform to an open circuit at the last slot. The shunt admittance of these terminations then vanishes at the last slots and so does not affect the input impedance. Mutual impedance terms to characterize the interaction among slot elements are not included in the basic design. The slotted waveguide is then described by the equivalent network in figure 2(b), where each slot is represented as a pure shunt conductance.

The element excitation is proportional to this slot conductance controlled by the displacement from the broadface centerline, x_e, according to [5]

$$g_e = 2.09 \frac{\lambda_g}{\lambda_0} \frac{a}{b} \cos^2\left(\frac{\pi\lambda_0}{2\lambda_g}\right) \sin^2\left(\frac{\pi x_e}{a}\right) \qquad e = \{1,\ 2,\ \ldots\ ,\ 10\}\ . \qquad (1)$$

The input to each waveguide arm is located between two radiating slots, so the coupling slot is a distance of $\lambda_g/4$ from the first radiating slot to the left and to the right. Then the impedance to the left and right of the input is transformed through quarter-wavelength sections and so has the same

Figure 2. Slotted waveguide antenna (a) front view (not to scale) showing coordinate system and (b) equivalent circuit (all elements not shown).
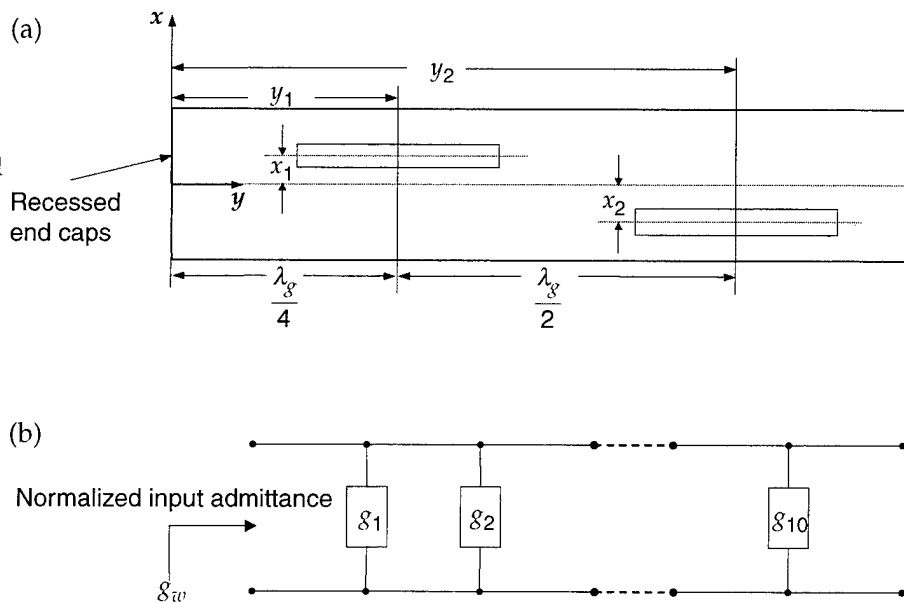
normalized values as the left and right conductance transformed to these slots closest to the input. Since the transformer coupling model is in series at the feed point, we have $z_L + z_R = 1$ or $g_L + g_R = 1$ so that the sum of all slot conductances is unity at the center frequency. The total normalized conductance at the input to each of the waveguide arms is then

$$g_w = \sum_{e=1}^{e=10} g_e = 1 \tag{2}$$

when matched to the waveguide impedance at the design frequency. For the chosen taper, the slot displacements are calculated so that the normalized conductance of all slots sums to unity for impedance matching at the center frequency. The phase of the slot excitation is that of the waveguide fields with phase constant $\beta = 2\pi/\lambda_g$, which would then be in phase at λ_g spacing. The radiating elements are alternated across the waveguide broadface centerline so that the slot excitation takes on alternating positive and negative values. This compensates for the out-of-phase condition introduced by the resonant spacing at $d_s = \lambda_g/2$. The slot's center positions and displacement for an S-band array module are shown in table 2. The modules have identical slot elements, except that they are symmetric about the array center, with the largest slot displacements located at the array center.

The array requires equal distribution of the input power, $P_{IN} = 25$ MW, to each of the four modules, so the branch arm power $P_B = P_{IN}/4$ (see fig. 1(c)). This power is distributed to the waveguide arms ($w = 1 - 10$) and then to the slot elements ($e = 1 - 10$) according to the array excitation taper. For nonsymmetric limits in the array geometry, the power distribution function is a sine squared on a pedestal of height 0.177,

$$f(e) = 0.177 + (1 - 0.177) \sin^2 \left(\frac{e-1}{18} \pi \right) \qquad e = \{1, 2, \ldots, 10\} \ . \tag{3}$$

This excitation function concentrates power near the array center ($e = 10$ and $w = 10$). The minimum slot width, $w_e^{min} = 0.123$ in. (123 mil), is calculated based on the power distribution as will be described in section

Table 2. Position of slot centers on waveguide arms for an S-band array module.

Slot number e	Displacement from center x_e (in.)	Distance from outside edge y_e (in.)
1	0.133	1.571
2	0.141	4.587
3	0.162	7.604
4	0.191	10.620
5	0.222	13.637
6	0.252	16.653
7	0.278	19.670
8	0.298	22.686
9	0.313	25.702
10	0.320	28.719

2.2.2. The analysis assumes that the waveguide arms receive the maximum power from the feed arms. The actual slot width is larger than w_e^{min}, since thin slots become more difficult to machine accurately. The chosen slot width is 3/16 in. or $w_e = 0.1875$ in. (187.5 mil), which provides a design margin associated with the array power-handling capabilities. This slot width is somewhat larger than desired, since the ratio $l_e/w_e \sim 11$ is barely sufficient to approximate a thin slot (i.e., an ideal dipole) as used in the array calculations.

The slot resonant length corresponds to a frequency where the slot admittance becomes a pure conductance, and this length can be changed by the slot shape (or fatness) factor and/or the slot displacement from the waveguide centerline. The slot resonant length determines the pattern BW defined as the frequency range over which the antenna gain is at least half (i.e., 3 dB) the peak gain. The perturbation caused by the slot displacements is small, where an order of magnitude change in position produces a variation in the resonant length of about 4 percent [6]. The slot lengths could have been adjusted based on empirical nomagraphs to obtain the resonant length for each position in the array [15]. This was not attempted, since systematic errors could be introduced during fabrication and the array would still require empirical adjustment for mutual coupling effects. Analysis indicates that a 4 percent reduction in the slot resonant length would shift the array pattern BW to a higher frequency (~2.98 GHz) than designed.

Mutual coupling effects are neglected in the basic design and are best investigated experimentally. These effects tend to modify the array impedance and so change the impedance BW, depending on the maximum allowable VSWR. The array should be well matched to the input waveguide characteristic (wave) impedance, and the impedance BW is the range of frequencies where the array VSWR is within specifications. The radiating slot elements are identical in the basic design, and empirical adjustment and/or impedance matching would be expected for specific applications. The mutual coupling between elements in different waveguide arms is negligible as in collinear dipoles. However, mutual coupling between nearby elements in the same waveguide arm is small but not necessarily negligible. The perturbation of the slot impedance associated with mutual coupling is about an 8 percent increase in slot conductance [7]. Analysis indicates that mutual-coupling effects in the waveguide arms will shift the impedance BW to a higher frequency (~2.9 GHz). Mutual coupling in the feed arms lowers the input impedance and shifts the array impedance BW to a lower frequency. The combination of these opposite trends raises the VSWR and shifts the impedance BW to a higher frequency. The perturbation of the slot resonant length shifts the array pattern BW to a higher frequency. Although these effects were neglected in the basic design, the combination of such perturbations could lead to performance as designed. Then the final design implementation and incorporation of tuning and/or impedance matching elements will depend on an empirical evaluation of the as-fabricated array.

2.2.2 Feed Structure

The slotted-waveguide arms are used to form a planar array in four symmetric modules of 100 slots (see fig. 1(b)) or 400 total elements (see fig. 1(a)). The 1/8-in. brass end caps are recessed 1/16 in., which has been accounted for consistently throughout the array design and fabrication. Each slotted-waveguide arm ($w = 1 - 10$) is fed near the center by an inclined coupling slot in the waveguide rear face as shown in figure 3(a). In each array module, these slots are covered by a three-sided corporate-feed waveguide with standard WR-284 rectangular flange input as shown in figure 3(b). The coupling-slot angle provides the excitation taper perpendicular to the waveguide arms corresponding to the E-plane (i.e., vertical or elevation) radiation pattern. Mutual-coupling effects in the feed arms lower the feed-arm impedance and shift the array impedance BW to a lower frequency (~2.75 GHz) than designed.

A module is assembled from 10 slotted waveguides, which align the recessed channel and coupling slot previously milled into the rear of each waveguide. The three-sided WR-284 feed waveguide, fabricated by removing one narrow wall, is soldered into the recessed channel (40-mil deep) on the rear of the modules. A three-sided feed section is required so that the coupling slots are cut in only one surface. Otherwise, any mismatch in the aspect of slots in the two mating surfaces could severely degrade the array efficiency and power handling. The recessed channel at a depth of 40 mil compensates for the three-sided waveguide to produce the same interior dimension as standard WR-284. The corporate-feed waveguide is terminated at each end with end caps (i.e., short-circuit terminations). These 1/8-in. end caps are half-recessed as in the standard waveguide and located at $\lambda_g/2$ from the last coupling slot. Then at the last slots, the transformed load impedance is also a short circuit and so does not contribute to the series impedance.
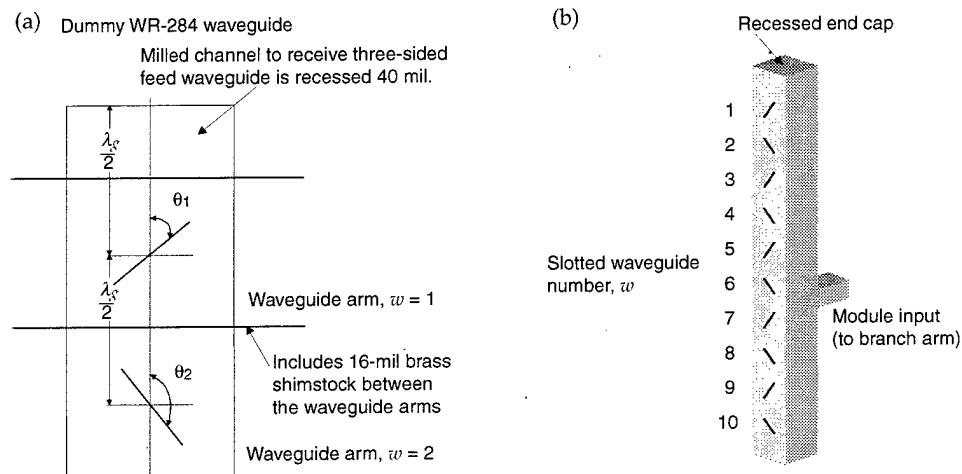

Figure 3. Feed-arm geometry with (a) coupling slots at alternating angles qw in rear face of waveguide arms and (b) three-sided feed-arm nomenclature with module input between waveguide arms $w = 6$ and $w = 7$.

10

Power Distribution

The input power is assumed to be equally distributed to the branch arms (see fig. 1(c)). This power is then distributed to the waveguide arms according to the excitation taper in equation (3). With conductor and mismatch losses neglected, the sum of the power to each waveguide arm is the branch arm power. The power actually fed to a module, P_M, by the corresponding branch arm can be estimated by

$$P_B = \sum_{w=1}^{w=10} P_w^W = P_1^W + P_2^W + \cdots + P_{10}^W \equiv P_M \sum_{w=1}^{w=10} f(w) = 5.89 P_M \ , \quad (4)$$

where $f(w)$ is the sine-squared distribution given by equation (3). The maximum power fed to the waveguide arms is closest to the array center or

$$P_w^{\max} = P_{10}^W = f(10) P_M = P_M = \frac{P_{\text{IN}}}{23.56} = 1.06 \ \text{MW} \quad (5)$$

for 25-MW-peak input power. Similarly, the maximum power in the center waveguide arm is distributed to the radiating elements according to

$$P_w^{\max} = \sum_{e=1}^{e=10} P_e^E = P_1^E + P_2^E + \cdots + P_{10}^E \equiv P_N \sum_{e=1}^{e=10} f(e) = 5.89 P_N \ . \quad (6)$$

The maximum power will be at element 10, so $P_e^{\max} = P_N = P_w^{\max}/5.89 = 180$ kW is the maximum power (peak) seen by a slot in the array.

Power Handling

If one assumes a uniform electric- (E-) field distribution in the aperture, $E(x,y) = E_s$, the slot voltage is $V_s = w_e E_s$, and the radiated power depends on the slot radiation conductance, $P_s = V_s^2 G_s$. The slot radiation conductance is determined by duality from the equivalent resonant dipole radiation resistance, $R_d = 73.2 \ \Omega$, by [15]

$$G_s = \frac{1}{R_s} = \frac{4R_d}{Z_0^2} = 4\frac{73.2 \ \Omega}{(120\pi)^2 \ \Omega^2} = 2.06 \ \text{mS} \ . \quad (7)$$

The maximum allowable E_s corresponds to the onset of air breakdown, $E_{\text{arc}} = 30$ kV/cm, and the maximum radiated power is $P_e^{\max}$. So the minimum slot width required to avoid air breakdown is given by

$$w_e^{\min} = \sqrt{\frac{Z_0^2 P_e^{\max}}{4R_d E_{\text{arc}}^2}} = \sqrt{\frac{(120\pi)^2 \ \Omega^2 \ 180 \ \text{kW}}{4(73.2 \ \Omega)(30 \ \text{kV/cm})^2}} = 0.312 \ \text{cm} = 123 \ \text{mil} \ . \quad (8)$$

We choose $w_e = 0.476$ cm $= 187$ mil as a trade-off between the minimum slot width and a convenient bit size (3/16 in.). Thus, the array power handling is not limited by air breakdown in the slot elements. The power-handling limits for the S-band waveguide are such that pressurization of the source waveguide is required and pressurization of the branch arms is needed, depending on the average power-handling requirement [16].

The inclined coupling slots present the impedance of the slotted-waveguide arms to the feed arm as a series impedance. The coupling then is series-series according to the coupling-slot transformer relations that transform the waveguide arm input impedance to an equivalent series impedance in the feed arm. The feed-arm inclined slot angles provide the excitation distribution and so the pattern characteristics in the E-plane. For broad-face slots, the impedance is normalized to the waveguide impedance and is proportional to the incline angle, θ_w, from the waveguide centerline (see fig. 3(a)). Mutual coupling in the feed waveguide is neglected in the basic design, since the coupling slots do not interact within the waveguide arms and multiple reflections in the feed arm are neglected. The equivalent impedance has a reactive component with the same magnitude for equal length slots (i.e., independent of angle). The inclined-slot normalized impedance can be written as $z_w = rw \pm j\alpha$, where the sign corresponds to positive or negative angles with respect to the feed waveguide centerline. The electrical equivalent shown in figure 4(a) is a transmission line with series impedances that represent the electrical equivalent of waveguide arms (as seen through the coupling transformers).

The orientations of the inclined slots are staggered across the feed-arm centerline to provide cancellation in pairs of the slot reactance. The phase of the coupling-slot excitation is that of the feed waveguide with phase constant $\beta = 2\pi/\lambda_g$ designed to be the same as WR-284. The coupling slots would be in phase at λ_g spacing, so alternating the slot orientation for each

Figure 4. Feed-arm equivalent circuit where (a) coupling-slot impedances on each side of input are in series and (b) parallel combination is feed-arm input impedance.
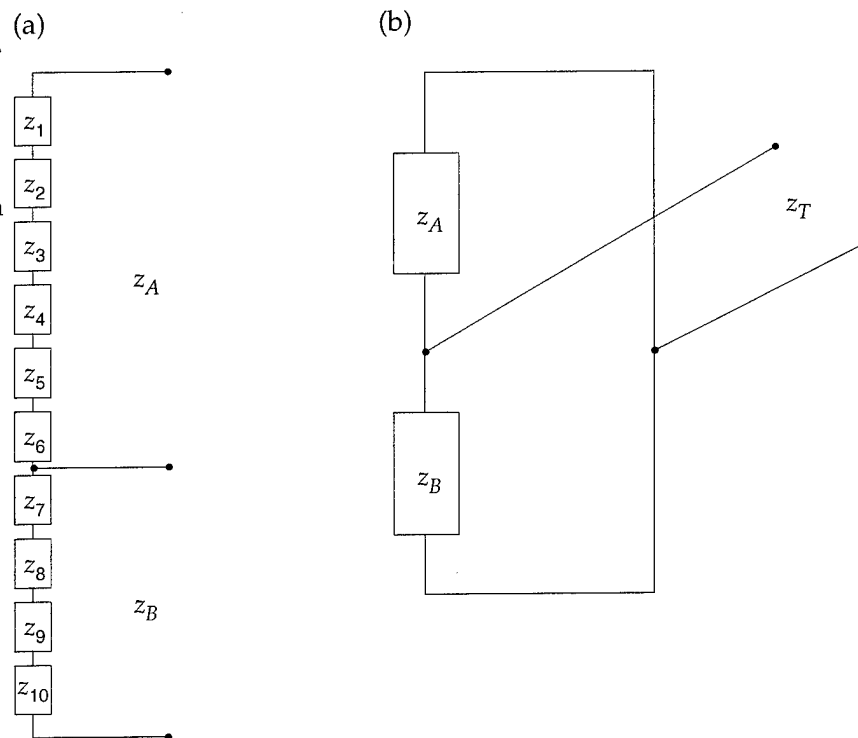
row waveguide compensates for the out-of-phase condition introduced by the resonant spacing. The real part of the coupling-slot impedance depends on the incline angle according to [15]

$$r_w = 0.131 \frac{\lambda_0}{\lambda_g} \frac{\lambda_0^2}{ab} \left[I(\theta_w) + \frac{\lambda_g}{2a} J(\theta_w) \cos \theta_w \right]^2 , \qquad (9)$$

where

$$\left. \begin{array}{c} I(\theta_w) \\ J(\theta_w) \end{array} \right\} = \frac{\cos\left(\frac{\pi\xi}{2}\right)}{1-\xi^2} \pm \frac{\cos\left(\frac{\pi\eta}{2}\right)}{1-\eta^2} \quad \text{and} \quad \left. \begin{array}{c} \xi \\ \eta \end{array} \right\} = \frac{\lambda_0}{\lambda_g} \cos\theta_w \mp \frac{\lambda_0}{2a} \sin\theta_w . \quad (10)$$

The incline angles for each 10-element feed arm are adjusted to provide the desired taper characteristics, while the input impedance is matched to the waveguide impedance.

The inclined slot impedances combine in series on each side of the feed-arm input as shown in figure 4(a). Since the series reactance cancels in pairs, the coupling-slot normalized impedance at the top (z_A) and at the bottom (z_B) is a pure resistance, or

$$z_A = \sum_{n=1}^{n=6} r_n \pm j\alpha_n = \sum_{n=1}^{n=6} r_n \equiv r_A \quad \text{and} \quad z_B = \sum_{n=7}^{n=10} r_n \pm j\alpha_n = \sum_{n=7}^{n=10} r_n \equiv r_B . \qquad (11)$$

For negligible reactance, higher-order modes are not excited and mutual interactions between coupling slots in the feed arms are negligible. Referring to figure 4(b), the feed-arm input impedance is the parallel combination of the impedance on each side of the input, and this total input impedance, z_T, is matched to the waveguide impedance. The total normalized impedance looking into the feed-arm input (at elements 6 and 7 of fig. 4) is

$$z_T = \frac{z_A z_B}{z_A + z_B} = \frac{r_A r_B}{r_A + r_B} \equiv C r_T = 1 . \qquad (12)$$

Here, $C = 1/1.3269$ is a normalization factor, depending on the coupling-slot transformer ratios, applied to the desired taper value to obtain a matched input. All four of the feed arms are identical and positioned symmetrically on the array backplane (see fig. 1(a)) so that the largest coupling (i.e., $\theta_w \sim 45°$) is near the array center ($w = 10$). The results of the transmission-line analysis for the S-band feed arm are shown in table 3 corresponding to the transformed taper values required to obtain the desired taper.

Since the WR-284 waveguide has wall thickness $\delta_s = 80$ mil, the coupling slots feeding each waveguide arm cannot be positioned at the resonant spacing $d_w = \lambda_g/2$ when stacking the WR-284 to form the array module. However, the physical separation is less than the required separation so that shims between the slotted waveguide are used to obtain the resonant physical separation. WR-284 is used to fabricate the feed arm with 16-mil brass spacers inserted between the waveguide arms during final assembly of the array modules. One can easily fabricate the S-band array

13

Table 3. Feed-arm coupling-slot angles for an S-band array fabricated in WR-284.

Element number	Desired taper value	Normalized taper value	Inclined angle (°)	Adjusted angle (°)
1	0.1770	0.1334	+15.0	+15.0
2	0.1993	0.1502	−16.0	+106.0
3	0.2638	0.1988	+18.6	+18.6
4	0.3634	0.2739	−22.2	+112.2
5	0.4875	0.3674	+26.3	+26.3
6	0.6225	0.4691	−30.4	+120.4
7	0.7538	0.5681	+34.4	+34.4
8	0.8672	0.6535	−37.9	+127.9
9	0.9504	0.7162	+40.5	+40.5
10	0.9944	0.7494	−42.0	+132.0

Equivalent circuit		
Parameter	Value	Normalization
r_A	2.1135	1.5927
r_B	3.5658	2.6872
r_T	1.3269	1.0000

using only the WR-284 waveguide, since the three-sided feed-arm waveguide (mounted to the rear of the modules in a recessed channel) is easily fabricated from the standard WR-284.

The performance of the corporate-feed structure represents the largest uncertainty in the array design. The analysis resulting in equation (12) is sensitive to small errors in the waveguide impedance that is transformed by the coupling slots. The effect is to introduce an asymmetric input reactance that could increase the impedance mismatch and reduce efficiency. Furthermore, asymmetries within the feed arm result in phase errors in the array module excitation that corrupt the E-plane radiation pattern. An idealized analysis indicates the following general trends:

- The perturbed-slot resonant length shifts the array resonance (i.e., pattern BW) to a higher frequency.

- The effect of mutual coupling in the waveguide arms shifts the array VSWR minimum (i.e., impedance BW) to a higher frequency.

- The effect of mutual coupling in the feed arms shifts the feed-arm VSWR minimum to a lower frequency.

These trends can be dependent, and the combined effect cannot be completely quantified by analysis. In particular, the combined influence of these perturbations could lead to a reasonable array performance. Thus, the array is fabricated according to the basic design, with design modifications based on empirical results.

3. Fabrication and Assembly

Refurbished copper waveguide in a like-new condition is used throughout the antenna array, where the tolerance on wall thickness is ±5 mil [16]. For the S-band array, the manufacturing tolerance must be ±5 mil and the inclined angle of the coupling slots is specified with a tolerance of ±0.2°. Fabrication errors will primarily increase the SLL, but in practice, it has been found that errors that are completely random (and independent) will not significantly degrade the performance of large arrays [9–11]. However, systematic errors in machining the slotted waveguide can compound to large errors in the as-fabricated array. For the slot displacements off the waveguide axis, systematic errors must be in thousandths of a wavelength (±4 mil), which is consistent with the manufacturing tolerance. A fabrication error in the slot lengths is more critical when systematic errors in ten-thousandths of a wavelength (±0.4 mil) can lead to errors in the radiation pattern. For this reason, the slots all have an identical length that is accurately reproduced with the use of NC milling operations. Systematic errors in the slot positions lead to asymmetries that produce phase errors and can enhance the amplitude of second-order beams [12]. Even small systematic errors can drastically degrade performance, and for a given error, the degradation would increase (and become severe) as the number of array elements increases [17]. The specified tolerance for the S-band array could lead to a 1-dB increase in SLL for a systematic offset in the slot displacements. An almost 5-dB increase in SLL could cause a systematic error in the slot length [17]. Such systematic errors would not be expected in the milling operations, and the degradation in SLL associated with random manufacturing errors can be estimated as 0.5 dB [11].

The NC fabrication processes can produce the array parts with negligible systematic errors; however, extreme care must be taken in the assembly processes not to introduce additional errors. After the end caps are attached with solder, each module is assembled on a flat surface with 16-mil shims between the row waveguide and is clamped in all directions. Final assembly of the slotted-waveguide modules is done with the resin-core solder between each waveguide, including a dummy waveguide at the array top and bottom.

The feed waveguide is soldered to the rear of the module in the channel previously milled in each waveguide arm. In this manner, a smooth surface is provided that is shared between the module waveguide arms and the feed waveguide. This shared surface allows the inclined-coupling slots to be machined in only the rear of the waveguide arms for ease of fabrication and eliminates slot aspect alignment errors in the module assembly.

The overlapping feed sections in the middle of the array are soldered to the next module waveguide, forming left and right halves of the full array.

The array half-sections would be attached to a rigid frame with appropriate hardware. Here, we secure the modules to a temporary wooden frame for subsequent testing as can be seen in figure 5(a). The actual supporting structure would be designed to provide flexibility for fabrication of the source-system interface and for integration on mobile platforms.

Figure 5. S-band array (a) side view showing feed structure and mechanical support elements and (b) front view showing high-bay test configuration.

(a)
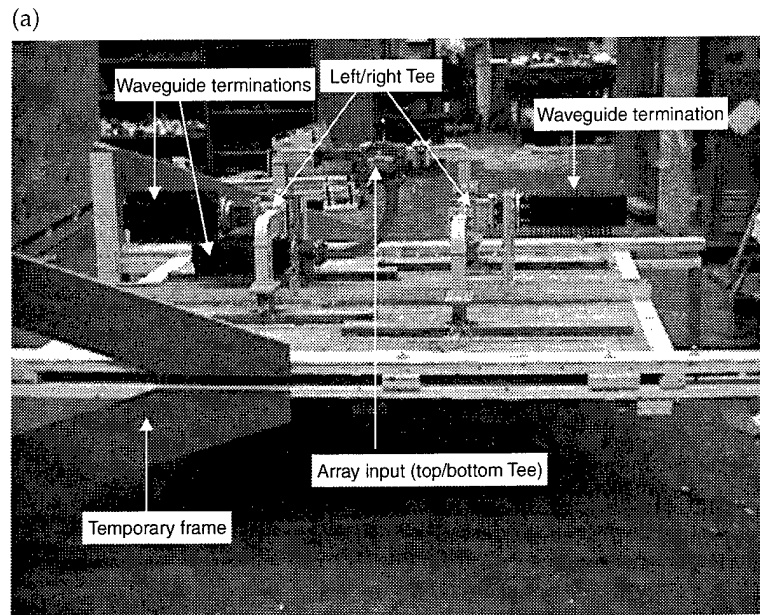
(b) Four-module array ($m = 1 - 4$)
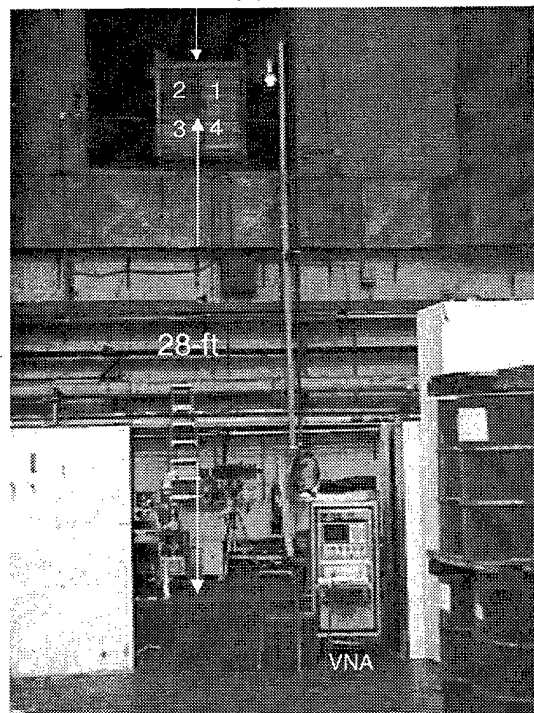
Fabrication of the S-band array required copper WR-284, brass end caps and shimstock, along with the solder and hardware required for final assembly of the array and feed network. The end caps and waveguide are both stepped to provide a 1/16-in. recess of the waveguide and allow good solder connections without contaminating the waveguide interior. The feed waveguide is a longer section of WR-284, constructed by removing one narrow wall. The three-sided feed has a height 40 mil larger than required so that when mounted in a 40-mil recessed groove, the feed waveguide has the same inside dimensions (hence the same λ_g) as a standard WR-284. After the WR-284 is fabricated, all parts are cleaned and tin-plated in a two-step bath process. Since a sufficient quantity of refurbished WR-284 was available, the material cost and lead time required for the S-band array were significantly reduced compared to the use of new materials. The fabrication costs are also lower, since custom parts were not required. With engineering labor costs neglected, the total estimated cost for fabrication and assembly of the S-band array is $35k ($19k for machining parts). The total estimated weight is 450 lb in a total volume of about 22 ft^3.

Fabrication of the feed network required additional WR-284 and standard S-band microwave components that were all refurbished in like-new condition. Flat rectangular cover flanges and waveguide seals (combination pressure and rf gaskets) were used throughout the feed network. This provides flexibility in connecting the feed network where the seals were also used as shims for final adjustment of the waveguide lengths. The required parts included six waveguide bends (two E-plane and four H-plane 90° bends) and three hybrid junctions, with matched terminations. Waveguide bends are used to position the junction terminations and mechanical support structures in a convenient location as can be seen in figure 5(a). The total cost is estimated as less than $8k, adding about 100 lb to the array weight, depending on the terminations used. The feed network increases the array depth to about 2 ft for a total array volume of less than 60 ft^3. The feed structure is adjusted to have approximately equal length; hence, in-phase branch arms from the waveguide are inputted to the module-input ports. This is accomplished empirically with the use of a short section of WR-284 and waveguide seals as convenient shims, taking care to maintain phase coherence through the waveguide junctions and corners. A photograph of the full-array test configuration (front view) is shown in figure 5(b).

4. Laboratory Test and Evaluation

Test and evaluation of a single array module is conducted immediately after final assembly. The results are used to refine the module fabrication/assembly procedures as required. The as-built performance of a single S-band array module ($m = 1$) was evaluated in the ARL anechoic chamber. Preliminary testing focused on the VSWR and main-beam characteristics with radiation pattern data taken in the principal planes. Of future interest are the power-handling limitations, the presence of second-order beams, the effectiveness of side-lobe suppression treatment options, and the impact of different radome structure options.

4.1 Single Module

A single S-band array module can be reliably evaluated in the ARL $20 \times 20 \times 50$ anechoic chamber. The test arrangement is shown in figure 6(a) with automated data acquisition at an angular resolution of $2.5°$, with the use of a Hewlett Packard (HP8510c) vector network analyzer (VNA). Calibration is accomplished with an S-band standard-gain horn antenna as shown in figure 6(b). Results at two frequencies (2.89 and 2.98 GHz) are shown in figure 7(a) and (b) for the H- and E-plane radiation pattern, respectively. The H-plane beamwidth is $7.6°$ with SLL > 15 dB, which indicates a systematic error in the radiating slot geometry. As previously mentioned, this systematic error is the incorrect physical slot length to be resonant at the design frequency. That is, the pattern BW is centered near 2.98 GHz so that the tapered excitation (designed for 2.856 GHz) does not provide 20-dB SLL at this frequency. The split beam in the E-plane data indicates a phase error
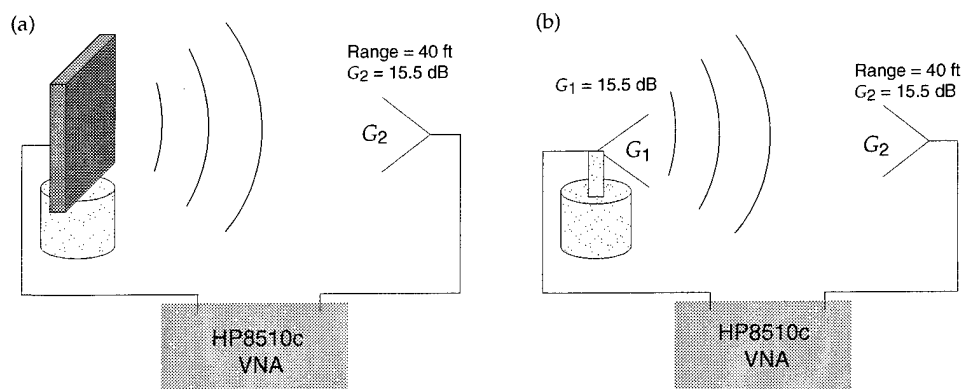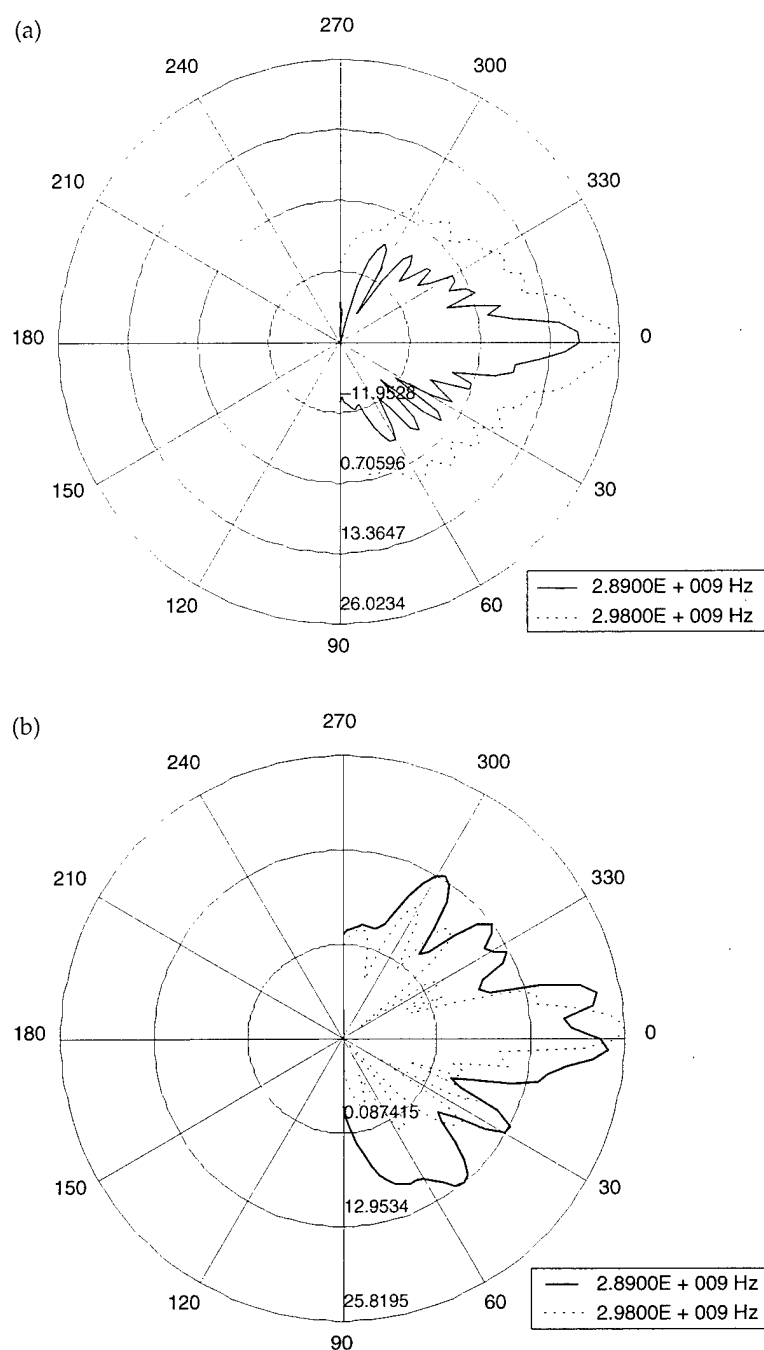

Figure 6. (a) Swept CW radiation pattern measurement with the use of a vector network analyzer (VNA) and S-band horn and (b) CW calibration measurement with the use of a VNA and S-band horns.

Figure 7. Measured
(a) H-plane realized gain at two frequencies showing peak gain on boresight and
(b) E-plane realized gain at two frequencies showing split-beam pattern.

in the corporate-feed waveguide, probably associated with asymmetries in the coupling-slot positions with respect to the feed point and/or end-cap terminations. The boresight gain as a function of frequency is shown in figure 8, indicating the shift in peak radiation (i.e., pattern BW) to a higher frequency (2.98 GHz). This is due to the shift in the resonant slot length that is correctable by adjusting the physical slot length. The next largest peak in the boresight gain versus frequency occurs at 2.89 GHz, corresponding to the impedance BW shifted to higher frequencies.

19

Figure 8. Measured gain on boresight showing peak radiation at 2.98 GHz.
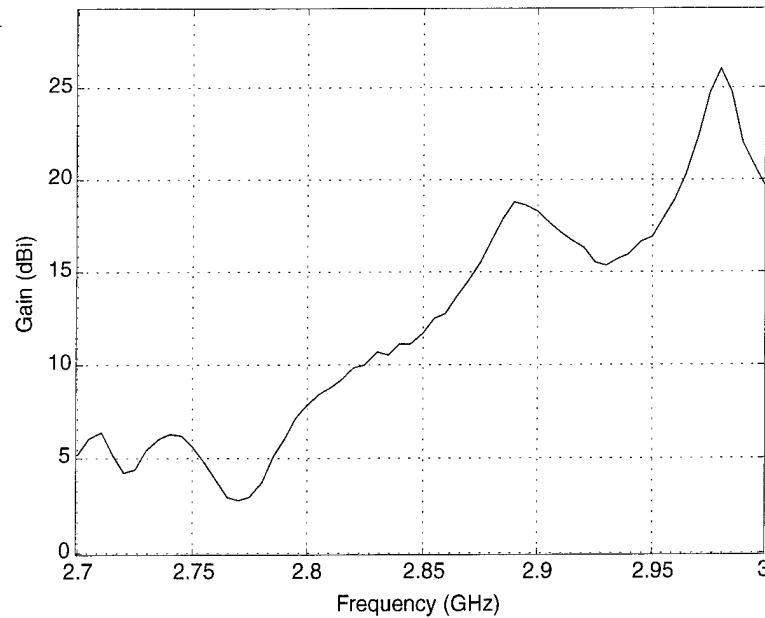
The measured VSWR versus frequency is shown in figure 9 for a single array module ($m = 1$). The data indicate that the single-module impedance BW is shifted to a higher frequency ($\sim$2.92 GHz). The VSWR data imply that the input impedance is not as expected at the design frequency, probably because of mutual coupling in the waveguide arms. The array minimum VSWR is shifted to a higher frequency and, at this frequency, is somewhat larger than desired, probably because of mutual coupling in the feed arms. As expected, the array input impedance is an extremely narrow band, but a minimum VSWR is obtained at two frequencies. The array input better matches the waveguide impedance at a higher frequency than designed, depending on mutual coupling effects. For the array operated at this frequency, the radiating slots are not yet resonant so that the array input impedance is not matched. The combined effect is a gain versus frequency result that has peak radiation at 2.89 GHz as shown in figure 8. The slot resonance is shifted to a higher frequency because of the perturbed slot resonant length, but at this frequency, the module-input impedance is not designed to match the waveguide impedance. The slot physical lengths would be adjusted as required to lower the slot resonant frequency and align the pattern BW with the impedance BW near 2.9 GHz.

For comparison, the predicted VSWR for an idealized array module (and the full array) is shown in figure 10(a). The results are in qualitative agreement to the measured VSWR, except for the frequency shift and the second minimum corresponding to the shifted slot resonant frequency. The mutual coupling to nearby radiating elements tends to increase the slot conductance (or reduce the element excitation for the same input power) and so primarily affects the input VSWR (or efficiency). Based on empirical data for a similar slotted waveguide, an 8 percent increase in slot conductance could be associated with mutual-coupling effects in the waveguide arms. Similarly, an 8 percent decrease in feed-arm input impedance could

20

Figure 9. Measured
VSWR for a single
module of S-band array.
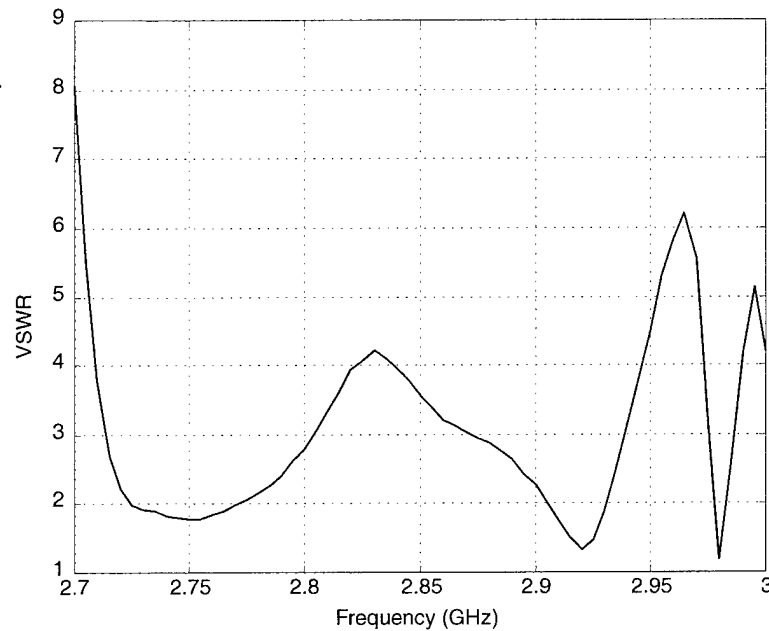
be associated with mutual coupling in the corporate-feed waveguide. The perturbed impedance results in the VSWR shown in figure 10(b). This calculation indicates that mutual-coupling effects would result in a matched input at a higher frequency, which is apparent in the measured data. The VSWR data then indicate that the array has impedance BW that depends on mutual-coupling effects. Furthermore, the slot resonant length is perturbed, resulting in another minimum VSWR at the resonant frequency. The adopted approach is to empirically adjust the geometry of a few slots near the array center (and use impedance-matching circuits as required) to obtain optimum performance in a given application (i.e., frequency range). The estimated attenuation caused by conductor losses in all four modules for the VSWR (including mutual coupling) versus frequency is shown in figure 10(c). The total attenuation for the full array corresponds to 50 m of WR-284 copper waveguide (i.e., 0.02 dB/m loss per unit length) with a minimum attenuation of $\sim$1 dB.

4.2   Full Array

The size of the full array precluded an accurate pattern characterization as a sufficiently large anechoic chamber (or antenna range) was not available. We conducted a preliminary evaluation by measuring the main-beam characteristics in a large building (see fig. 5(b)). The test arrangement is shown in figure 11 with calibration accomplished with standard-gain matched horn antennas as in the anechoic chamber measurements. In these measurements, the horn antenna is mechanically positioned where the angular range is limited by the building size. Data are collected at an angular resolution of 1° with an experimental error $\sim$0.5 dB, although positioning error can increase the total uncertainty in the data. The feed system was first adjusted (to an accuracy of 1/16 in.) to have equal physical-length branch

Figure 10. (a) Calculated
VSWR for corporate
feed, a single module
and full array;
(b) calculated VSWR
including mutual
coupling, assuming an
8 percent impedance
reduction; and
(c) calculated total
attenuation caused by
conductor losses using
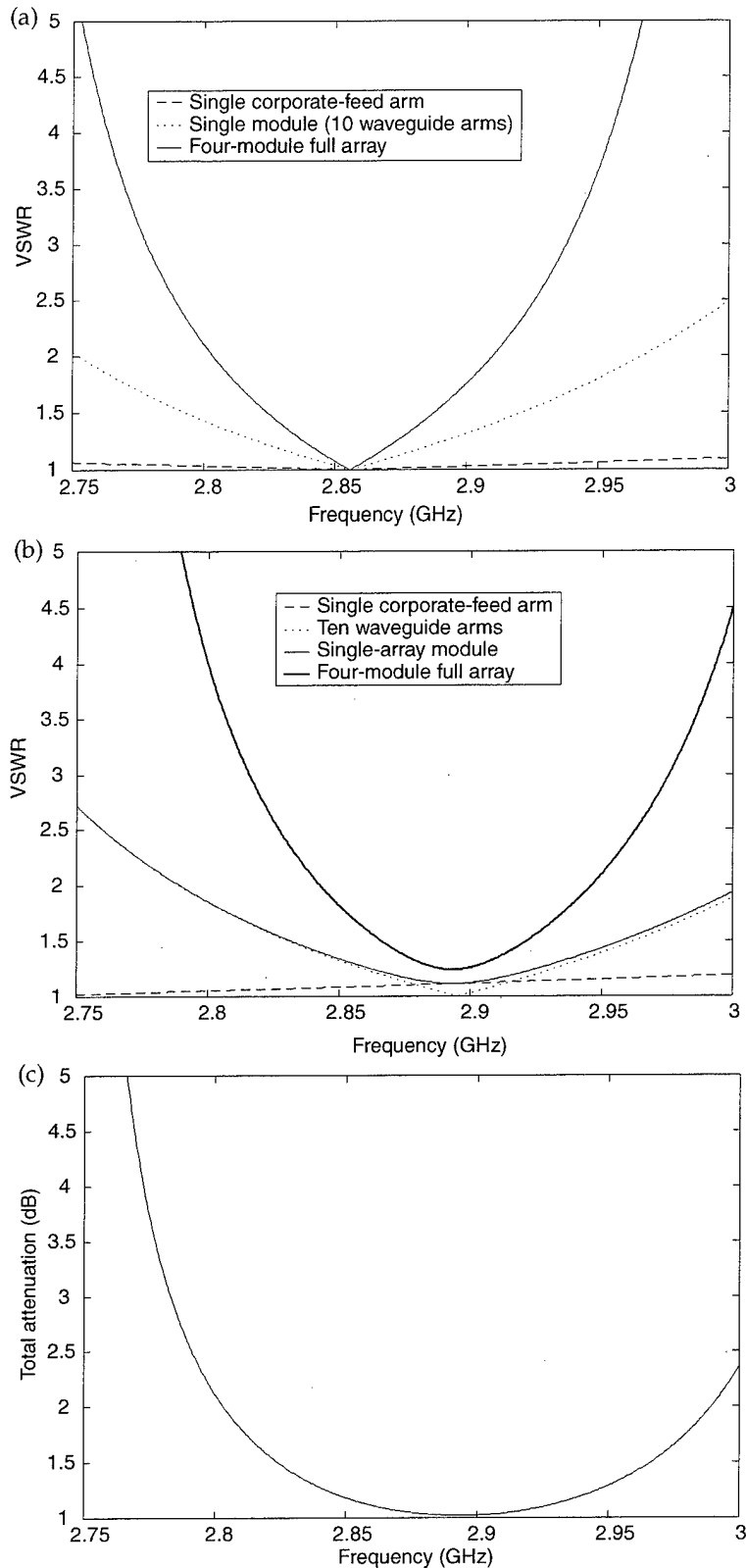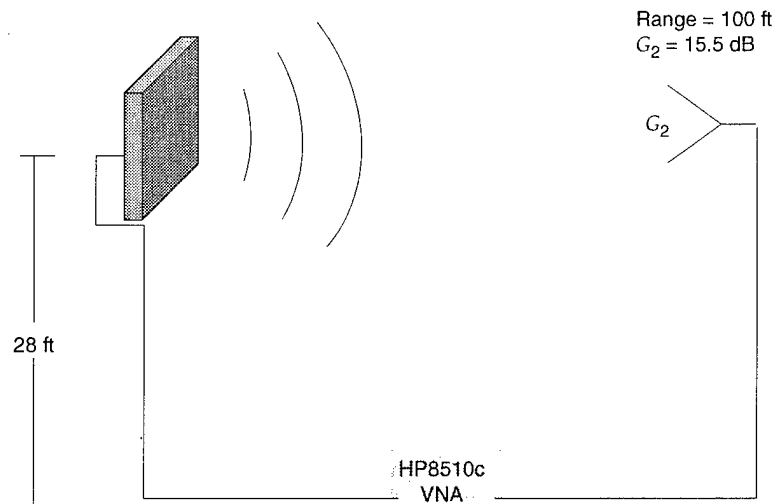VSWR of figure 10(b).

22

Figure 11. Physical configuration for antenna pattern measurements on four-module S-band array.

arms. This is accomplished by adjusting the branch-arm physical lengths to minimize the phase difference in the measured response of the four identically terminated module ports. The reflection coefficient phase angle, ϕ_m, of each output in the terminated feed structure is measured separately versus frequency with all other outputs terminated in a matched load impedance. With the use of the module nomenclature adopted throughout this report, the absolute phase difference between the two top modules ($m = 1$ and $m = 2$) and the two bottom modules ($m = 3$ and $m = 4$) is shown in figure 12(a). The results indicate that the top portion of the array is in phase to ~2° while the bottom portion has a phase difference of ~8°, indicating a small H-plane phase error. The absolute phase difference between a module in the array top ($m = 2$) and bottom ($m = 4$) is shown in figure 12(b). The phase difference near the design frequency is ~15°, which is a sufficiently large E-plane phase error to produce a split-beam radiation pattern.

The measured broadside or boresight gain (i.e., normal to the planar array) versus frequency for the four-module array is shown in figure 13. The calculated radiation pattern for the H- and E-plane gain of a half-wave dipole array is shown in figure 14(a) and (b), respectively. Compared to the measured gain, the calculated result implies a maximum insertion loss of 1 to 1.5 dB, which is consistent with expectations (see fig. 10(c)). The measured VSWR for the terminated feed network is shown in figure 15(a) for each branch arm with all others terminated in a matched load impedance. The minimum VSWR is obtained near 2.89 and 2.95 GHz, indicating some impedance variations in the terminated feed structure.

The results for the full array are shown in figure 15(b), indicating reasonable impedance matching over narrow frequency bands near 2.92 and 2.97 GHz. The measured H- and E-plane patterns at two frequencies over a limited angular range are shown in figure 16(a) and (b), respectively. The pattern corresponds to the full-array taper, so it is closer to the desired pattern than that produced by a single module near the boresight. However, the SLL indicates a systematic error so that the physical length of the slots must

Figure 12. Absolute phase difference between (a) left- and right-side array modules and (b) top and bottom array modules.

(a)

Top array modules
Bottom array modules

$|\phi_3 - \phi_4|$

$|\phi_1 - \phi_2|$

Phase difference (°)

Frequency (GHz)

×10⁹

(b)

$|\phi_2 - \phi_4|$

Phase difference (°)

Frequency (GHz)

×10⁹
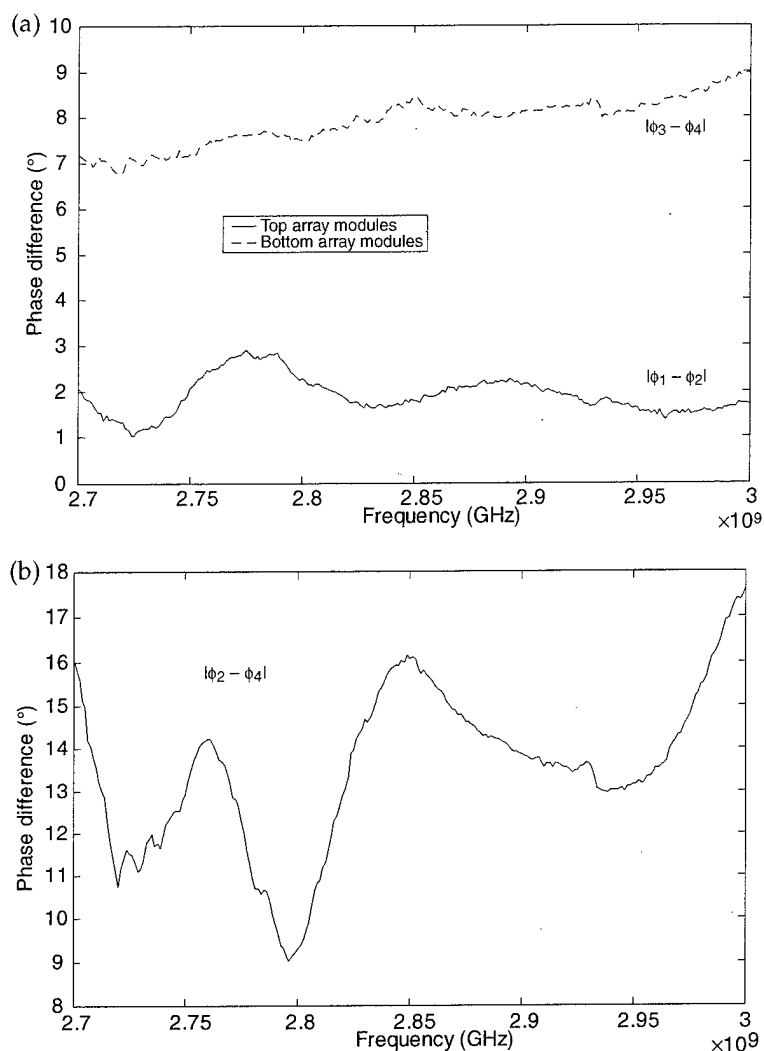
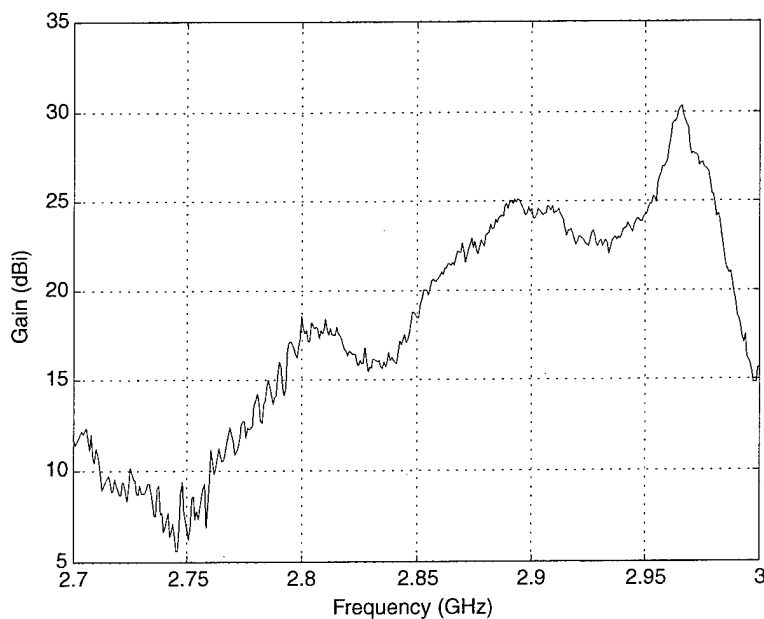Figure 13. Measured boresight gain of four-module full array showing peak radiation at 2.97 GHz.

Gain (dBi)

Frequency (GHz)

24

Figure 14. Calculated (a) H-plane and (b) E-plane radiation patterns for an array of resonant dipoles at 2.856 GHz.

(a)

Maximum gain = 31.4 dB
Beamwidth = 4.1°

Maximum gain = 25.4 dB
Beamwidth = 7.4°

Frequency = 2.856 GHz

—— Four-module array
—·— Single-module array

H-plane gain (dBi)

Azimuthal angle, ϕ (°)

(b)

Maximum gain = 31.4 dB
Beamwidth = 4.1°

Maximum gain = 25.4 dB
Beamwidth = 7.4°

Frequency = 2.856 GHz

—— Four-module array
—·— Single-module array

E-plane gain (dBi)

Elevation angle, θ (°)
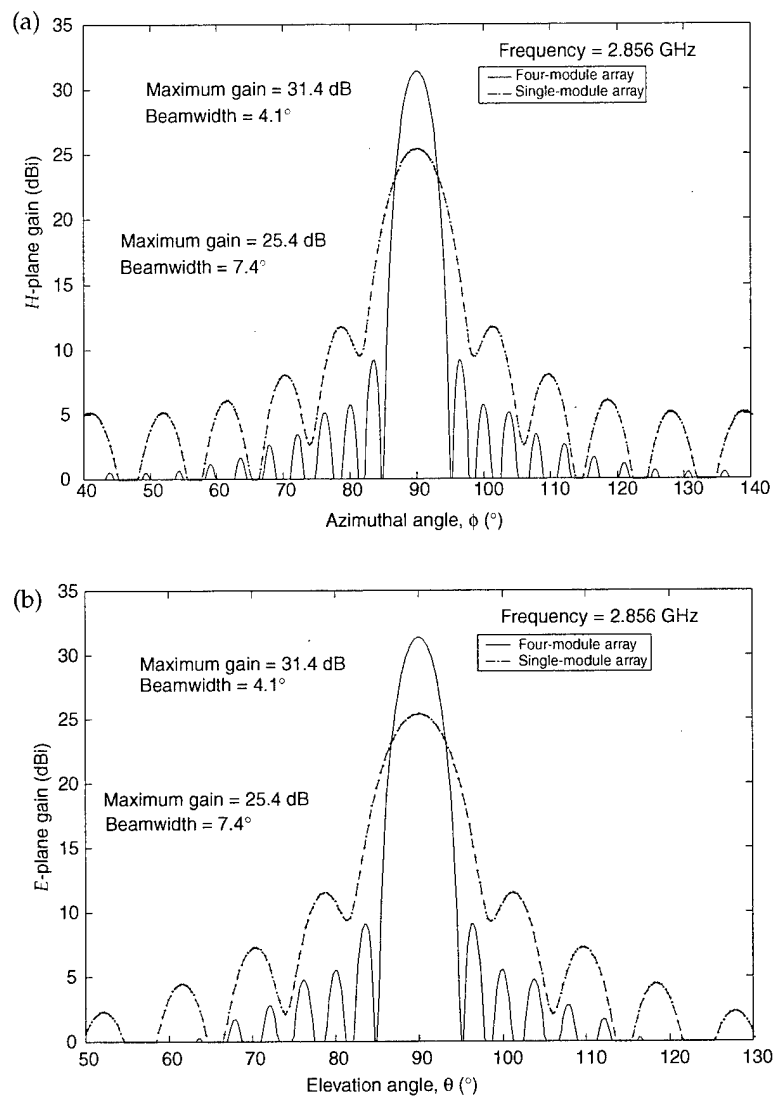
be adjusted to reduce the SLL. Empirical-based tuning of the slot lengths near the array center should bring the pattern BW (now at 2.97 GHz) closer to the impedance BW near 2.89 GHz. Empirical-based tuning of the array would be based on the measured VSWR as shown in figure 15(b).

Figure 15. (a) Measured VSWR for each output of feed structure with all others terminated and (b) measured input VSWR for four-module S-band array.
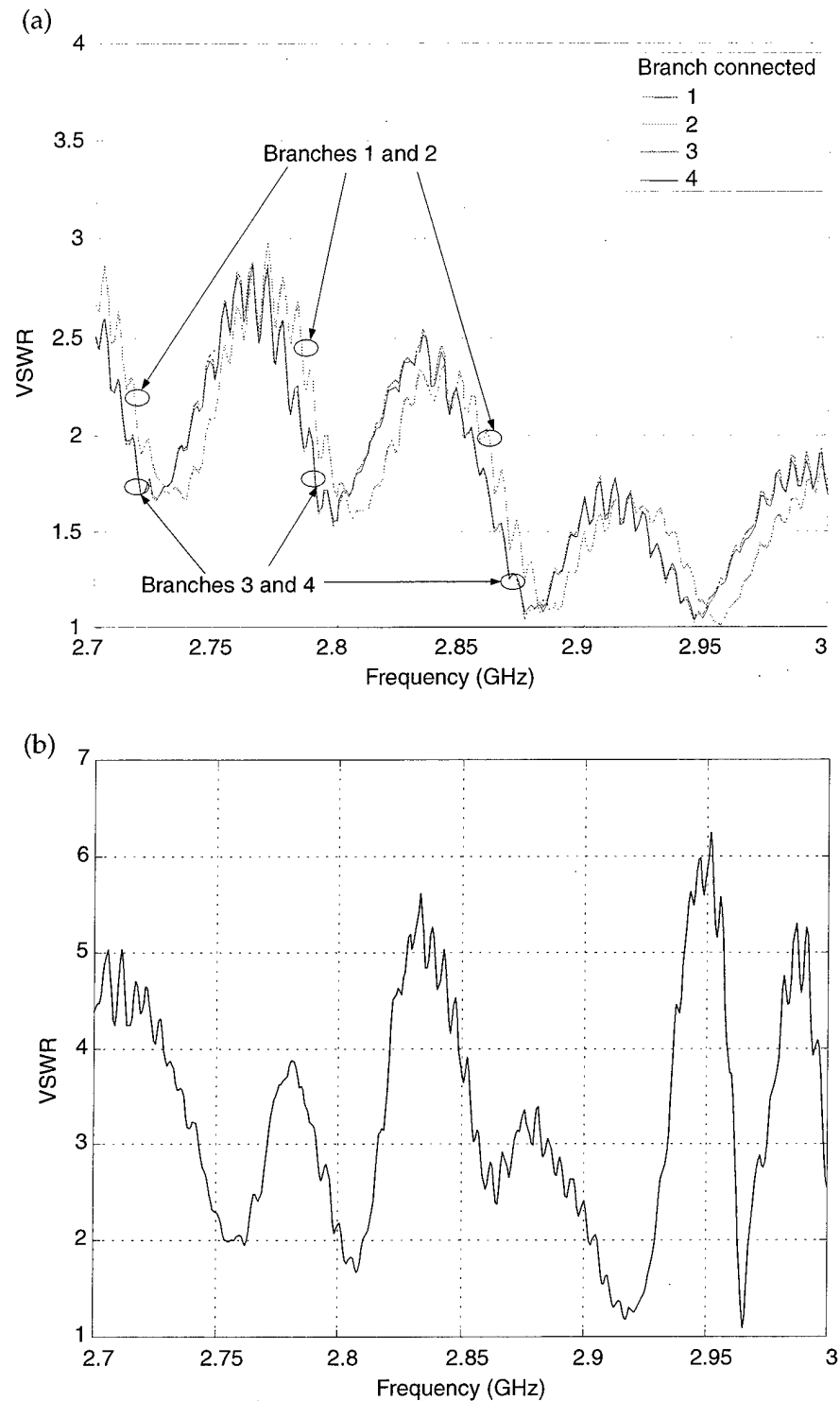
Figure 16. Measured
(a) *H*-plane and
(b) *E*-plane gains of
four-module array at
two frequencies for
angles near boresight.

(a)

Gain (dBi)

2.89 GHz
2.97 GHz

330

0

4.1996

7.1315

18.4627

29.7939   60

90

2.8898E + 009 Hz
2.9663E + 009 Hz

Elevation angle (°)

(b)

Gain (dBi)

2.89 Ghz
2.97 GHz

330

0

9.2763

14.5315

19.7867

25.0418

30.297   60

90

2.8898E + 009 Hz
2.9663E + 009 Hz

Azimuthal angle (°)
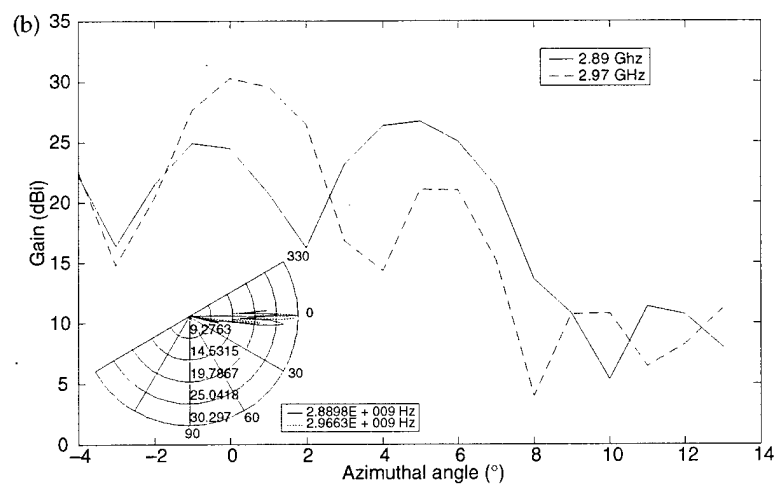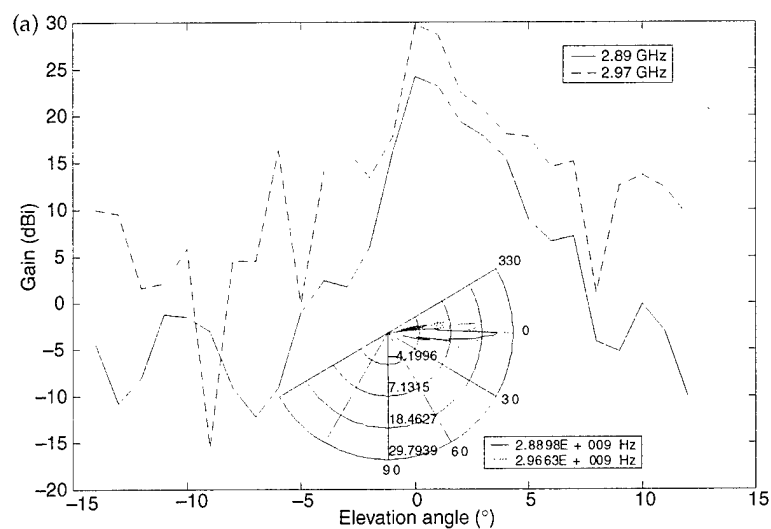
5. Conclusion

The preliminary results indicate that an S-band slotted-waveguide array can meet the desired performance objectives in terms of gain in a reasonable size and weight. The basic design requires modification to fully meet the operational requirements. At the array resonant frequency (2.97 GHz), the H-plane gain has a narrow beam on boresight as desired with the expected beamwidth. The beamwidth (to half-power points) is directly related to gain but is not well defined with only 1° angular resolution. The E-plane pattern has the expected peak gain with some beam splitting associated with the phase error between the array top and bottom sections. The array also has reasonable VSWR at 2.9 GHz, where the H-plane gain is reduced with a narrow beam pattern. The E-plane gain is also reduced at this frequency with a split beam pattern.

The phase error between array modules must be reduced to obtain the desired pencil beam-radiation pattern. This requires that the physical length of the branch arms be equal to an accuracy much better than 1/16 in. Empirical-based evaluation and modification of the array design are required to minimize such phase errors and obtain the desired resonant frequency. Some slots would be lengthened to lower the array resonant frequency, and the array should then have a lower SLL, as would be expected for the chosen array taper. The frequency range and SLL requirement were not adequately met by the basic array design. The design modifications are easily implemented, although SLL suppression treatments could be required, depending on the application. Based on VSWR, the impedance BW is extremely narrow unless a larger VSWR (e.g., 1.5 to 2) can be tolerated. Final evaluation of the array after optimization should be accomplished on a sufficiently large antenna range. The array power-handling ability and presence of second-order beams could then be investigated.

Acknowledgments

References

1. C. M. Glenn and S. T. Hayes, *High-Power Microwave Antenna Design— Phase 1 Status Report*, Fractal Dynamics (November 1997).

2. C. M. Glenn and S. T. Hayes, *High-Power Microwave Antenna Design— Phase 2 Status Report*, Fractal Dynamics (April 1998).

3. A. F. Stevenson, *Theory of Slots in Rectangular Wave-Guides*, J. Appl. Phys. **19** (January 1948), pp 24–38.

4. H. Gruenberg, *Theory of Wave-Guide-Fed Slots Radiating into Parallel-Plate Regions*, J. Appl. Phys. **23**, No. 7 (July 1952), pp 733–737.

5. A. L. Cullen, *Laterally Displaced Slot in Rectangular Waveguide*, Wireless Eng. (January 1949), pp 3–10.

6. R. J. Stegan, *Longitudinal Shunt Slot Characteristics*, Hughes Aircraft Company, Technical Memorandum, No. 261 (November 1951).

7. M. J. Ehrlich and J. Short, *Mutual Coupling Considerations in Liner-Slot Array Design*, Proc. IRE (June 1953), pp 956–961.

8. I. P. Kaminow and R. J. Stegan, *Waveguide Slot Array Design*, Hughes Aircraft Company, Technical Memorandum, No. 348 (July 1954).

9. L. L. Bailin and M. J. Ehrlich, *Factors Affecting the Performance of Linear Arrays*, Proc. IRE (February 1953), pp 235–241.

10. L. L. Bailin, *Fundamental Limitations of Long Arrays*, Hughes Aircraft Company, Technical Memorandum, No. 330 (October 1953).

11. H. F. O'Neil and L. L. Bailin, *Further Affects of Manufacturing Tolerances on the Performance of Linear Shunt Slot Arrays*, Hughes Aircraft Company, Technical Memorandum, No. 263 (1953).

12. H. Gruenberg, *Second-Order Beams of Slotted Wave Guide Arrays*, Can. J. Phys. **31** (1953), pp 55–69.

13. C. L. Dolph, *A Current Distribution for Broadside Arrays Which Optimizes the Relationship Between Beam Width and Side-Lobe Level*, Proc. IRE and Waves and Electrons (June 1946), pp 335–348.

14. W. L. Stutzman and G. A. Thiele, *Antenna Design and Theory*, John Wiley and Sons, Inc. (1981), pp 188 and 384.

15. Henry Jasik, ed., *Antenna Engineering Handbook*, McGraw-Hill Book Co. (1961).

16. Theodore S. Saad, ed., *Microwave Engineers' Handbook* **1**, Artech House, Inc. (1971).

17. Theodore S. Saad, ed., *Microwave Engineers' Handbook* **2**, Artech House, Inc. (1971).

Distribution

Admnstr
Defns Techl Info Ctr
ATTN DTIC-OCP
8725 John J Kingman Rd Ste 0944
FT Belvoir VA 22060-6218

DARPA
ATTN S Welby
3701 N Fairfax Dr
Arlington VA 22203-1714

Ofc of the Secy of Defns
ATTN ODDRE (R&AT)
The Pentagon
Washington DC 20301-3080

Ofc of the Secy of Defns
ATTN OUSD(A&T)/ODDR&E(R) R J Trew
3080 Defense Pentagon
Washington DC 20301-7100

AMCOM MRDEC
ATTN AMSMI-RD W C McCorkle
Redstone Arsenal AL 35898-5240

US Army TRADOC
Battle Lab Integration & Techl Dirctrt
ATTN ATCD-B
FT Monroe VA 23651-5850

US Military Acdmy
Mathematical Sci Ctr of Excellence
ATTN MADN-MATH MAJ M Huber
Thayer Hall
West Point NY 10996-1786

Dir for MANPRINT
Ofc of the Deputy Chief of Staff for Prsnnl
ATTN J Hiller
The Pentagon Rm 2C733
Washington DC 20301-0300

SMC/CZA
2435 Vela Way Ste 1613
El Segundo CA 90245-5500

TECOM
ATTN AMSTE-CL
Aberdeen Proving Ground MD 21005-5057

US Army ARDEC
ATTN AMSTA-AR-TD
Bldg 1
Picatinny Arsenal NJ 07806-5000

US Army Info Sys Engrg Cmnd
ATTN AMSEL-IE-TD F Jenia
FT Huachuca AZ 85613-5300

US Army Natick RDEC Acting Techl Dir
ATTN SBCN-T P Brandler
Natick MA 01760-5002

US Army Simulation Train & Instrmntn
   Cmnd
ATTN AMSTI-CG M Macedonia
ATTN J Stahl
12350 Research Parkway
Orlando FL 32826-3726

US Army Tank-Automtv Cmnd RDEC
ATTN AMSTA-TR J Chapin
Warren MI 48397-5000

Nav Surfc Warfare Ctr
ATTN Code B07 J Pennella
17320 Dahlgren Rd Bldg 1470 Rm 1101
Dahlgren VA 22448-5100

Hicks & Assoc Inc
ATTN G Singley III
1710 Goodrich Dr Ste 1300
McLean VA 22102

Pacific Northwest Natl Lab
ATTN K8-41 R Shippell
PO Box 999
Richland WA 99352

Palisades Inst for Rsrch Svc Inc
ATTN E Carr
1745 Jefferson Davis Hwy Ste 500
Arlington VA 22202-3402

Director
US Army Rsrch Lab
ATTN AMSRL-RO-D JCI Chang
ATTN AMSRL-RO-EN W D Bach
PO Box 12211
Research Triangle Park NC 27709

Distribution (cont'd)

US Army Rsrch Lab
ATTN AMSRL-D D R Smith
ATTN AMSRL-DD J M Miller
ATTN AMSRL-CI-AI-R Mail & Records
  Mgmt
ATTN AMSRL-CI-AP Techl Pub (2 copies)
ATTN AMSRL-CI-LL Techl Lib (2 copies)
ATTN AMSRL-SE-DP M Litz
ATTN AMSRL-SE-DP N Tesny

US Army Rsrch Lab (cont'd)
ATTN AMSRL-SE-DP L Dilks
ATTN AMSRL-SE-DP C Brown
ATTN AMSRL-SE-DS B King
ATTN AMSRL-SE-DS J Miletta
ATTN AMSRL-SE-DS W O Coburn
  (5 copies)
Adelphi MD 20783-1197

REPORT DOCUMENTATION PAGE

Public reporting burden for this collection of information is estimated to average 1 hour per response, including the time for reviewing instructions, searching existing data sources, gathering and maintaining the data needed, and completing and reviewing the collection of information. Send comments regarding this burden estimate or any other aspect of this collection of information, including suggestions for reducing this burden, to Washington Headquarters Services, Directorate for Information Operations and Reports, 1215 Jefferson Davis Highway, Suite 1204, Arlington, VA 22202-4302, and to the Office of Management and Budget, Paperwork Reduction Project (0704-0188), Washington, DC 20503.

1. AGENCY USE ONLY (Leave blank)	2. REPORT DATE January 2001	3. REPORT TYPE AND DATES COVERED Progress, FY 2000

4. TITLE AND SUBTITLE A Slotted-Waveguide Array for High-Power Microwave Transmission

5. FUNDING NUMBERS

DA PR: A140

PE: 62120A

6. AUTHOR(S) William Coburn, Marc Litz, Joseph Miletta, Neal Tesny, Lillian Dilks, Charles Brown, and Benson King

7. PERFORMING ORGANIZATION NAME(S) AND ADDRESS(ES)
U.S. Army Research Laboratory
Attn: AMSRL-SE-DS   email: wcoburn@arl.army.mil
2800 Powder Mill Road
Adelphi, MD 20783-1197

8. PERFORMING ORGANIZATION REPORT NUMBER
ARL-TR-2331

9. SPONSORING/MONITORING AGENCY NAME(S) AND ADDRESS(ES)
U.S. Army Research Laboratory
2800 Powder Mill Road
Adelphi, MD 20783-1197

10. SPONSORING/MONITORING AGENCY REPORT NUMBER

11. SUPPLEMENTARY NOTES
ARL PR: 0NEYYY
AMS code: 622120.140

12a. DISTRIBUTION/AVAILABILITY STATEMENT Approved for public release; distribution unlimited.

12b. DISTRIBUTION CODE

13. ABSTRACT (Maximum 200 words)

Directive antennas are required for the development of high-power microwave (HPM) transmission system concepts. The type of system considered includes a single HPM source with waveguide output, the antenna, and the control/support equipment integrated onto a ground-mobile platform. A parabolic reflector with a custom-designed horn feed has been demonstrated as one antenna option that allows direct connection to the HPM source waveguide output. An alternative approach to reflector antennas is desired, so a slotted-waveguide array was selected to meet the operational requirements. The array design is modular (with four symmetric modules) to ease fabrication and to maximize transportability and repairability. A rectangular waveguide corporate-feed network is used to minimize the antenna subsystem volume (i.e., depth) and allow the HPM source to be integrated into the feed structure. An S-band array and feed structure were fabricated and assembled for laboratory evaluation. The array was fabricated from WR-284 copper waveguide with brass end caps to a ±5-mil tolerance. The array design, fabrication, assembly, and testing are discussed. Preliminary test data for a single module of the four-module full array are presented. As expected, the array as fabricated requires "fine-tuning" to optimize performance. Empirical results will be used to evaluate design alternatives appropriate for particular HPM applications.

14. SUBJECT TERMS antenna array

15. NUMBER OF PAGES
40

16. PRICE CODE

17. SECURITY CLASSIFICATION OF REPORT	18. SECURITY CLASSIFICATION OF THIS PAGE	19. SECURITY CLASSIFICATION OF ABSTRACT	20. LIMITATION OF ABSTRACT
Unclassified	Unclassified	Unclassified	UL

NSN 7540-01-280-5500